Dual isotope measurements reveal zoning of nitrate processing in the summer Changjiang (Yangtze) River plume: Nitrate dynamics ....

Article *in* Geophysical Research Letters · November 2017

DOI: 10.1002/2017GL075951

7 authors, including:

Xiuli Yan
Xiamen University
7 PUBLICATIONS **49** CITATIONS
SEE PROFILE

Min Xu
Xiamen University
9 PUBLICATIONS **12** CITATIONS
SEE PROFILE

Jin-Yu Terence Yang
Pohang University of Science and Technology
17 PUBLICATIONS **260** CITATIONS
SEE PROFILE

Minhan Dai
Xiamen University
214 PUBLICATIONS **5,598** CITATIONS
SEE PROFILE

AGU PUBLICATIONS

Geophysical Research Letters

RESEARCH LETTER
10.1002/2017GL075951

Key Points:
- Three zones with different nitrogen processes were identified using isotopic composition, and these correspond to different physical regimes
- Primary producers in coastal waters utilized nitrate that has already been microbially altered and recycled
- Caution is required to derive biological isotope effects in a plume using the initial nitrate composition of the freshwater end-member

Supporting Information:
- Supporting Information S1

Correspondence to:
S.-J. Kao,
sjkao@xmu.edu.cn

Citation:
Yan, X., Xu, M. N., Wan, X. S., Yang, J.-Y. T., Trull, T. W., Dai, M., & Kao, S.-J. (2017). Dual isotope measurements reveal zoning of nitrate processing in the summer Changjiang (Yangtze) River plume. *Geophysical Research Letters*, *44*. https://doi.org/10.1002/2017GL075951

Received 18 JUL 2017
Accepted 10 NOV 2017
Accepted article online 13 NOV 2017

Dual Isotope Measurements Reveal Zoning of Nitrate Processing in the Summer Changjiang (Yangtze) River Plume

Xiuli Yan[1], Min Nina Xu[1], Xianhui Sean Wan[1], Jin-Yu Terence Yang[1], Thomas W. Trull[2], Minhan Dai[1], and Shuh-Ji Kao[1]

[1]State Key Laboratory of Marine Environmental Science, College of Ocean and Earth Sciences, Xiamen University, Xiamen, China, [2]Antarctic Climate and Ecosystems Cooperative Research Centre, University of Tasmania, and CSIRO Oceans and Atmosphere, Hobart, Australia

Abstract Riverine nitrogen input into the coastal zone has increased remarkably in recent decades. Yet its transformation and recycling within hydrodynamically active regions remains unclear. Using observations of nitrate concentration and dual isotopic composition across the Changjiang River plume within a three end-member mixing model, we found deviations between the observed and expected values for mixing alone, revealing the nonconservative behavior of nitrate. Using cross correlations between concentrations and dual isotope deviations, we identified three nitrogen transformation zones, which correspond to separate portions of the plume. Nitrification and sedimentary denitrification occurred near the river mouth, nitrification prevailed further offshore under the plume, and finally, phytoplankton assimilation occurred in the outer surface plume (>100 km offshore), where it was fueled by nitrate that had already been strongly modified by microbial processes. Information was assembled into a conceptual model offering an overview of nitrogen transformations in a large river plume.

1. Introduction

Estuaries and coastal oceans receive riverine nutrient inputs, which have significantly increased in recent decades (Gruber and Galloway, 2008; Sharples et al., 2017). Anthropogenic inputs have led to a host of environmental problems, such as harmful algal blooms, eutrophication, and seasonal hypoxia in estuaries and adjacent coastal areas (Anderson et al., 2002; Billen et al., 1999; Diaz & Rosenberg, 2008), interfering with the original functions of coastal ecosystems and biogeochemical cycles. Nitrogen (N) is also a pivotal element in regulating marine primary productivity (Moore et al., 2013), and consequently, its availability affects the sequestration of anthropogenic carbon dioxide in coastal and marginal seas. Thus, improving our ability to trace N sources, its recycling processes, and dispersal behavior in hydrodynamic plumes offers broad benefits.

The Changjiang river (CJ) provides the largest freshwater input into the East China Sea (ECS), with an average flow of 0.03 Sverdrup (1 Sverdrup = 10^6 m^3/s, reaching 0.05 Sverdrup during summer flood) placing it in the top five rivers globally. Its highly turbid plume extends >100 km offshore (Tseng et al., 2014), and it delivers increasingly large N inputs (Dai et al., 2011), which are detectable throughout the ECS (Umezawa et al., 2014). These N inputs contribute to seasonal hypoxia (in summer when the river flood peaks; Zhu et al., 2011) and harmful algal blooms (Li et al., 2014). The interaction of the CJ plume with coastal waters is complex, with strong gradients in turbidity/sedimentation and N biogeochemistry that are also modulated by regional currents (Figure 1a). In particular, the Nearshore Kuroshio Branch Current (NKBC) transports similar amounts of NO_3^- as CJ river to the CJ plume since it has a flow ~10-fold higher (0.4–1.0 Sverdrup) but NO_3^- levels ~10-fold lower than that of CJ (Chen, 1996; Tseng et al., 2014; Yang et al., 2012). Using the stable carbon isotope ($\delta^{13}C$) combined with a three end-member model, Wang et al. (2016) demonstrated that the summer hypoxia in bottom waters of CJ plume could be attributed to decomposition of biomass produced by overlying phytoplankton. On the one hand, the intensive remineralization beneath the plume can be another NO_3^- source to the CJ plume. On the other hand, denitrification in the sediments may lead to N loss (Song et al., 2013), particularly in summer when DO (dissolved oxygen) levels are lowest. Thus, under such complex hydrodynamic conditions and intensive biological activities, what are the dynamics of and biogeochemical controls on the NO_3^- distribution across the CJ plume? Can we assess

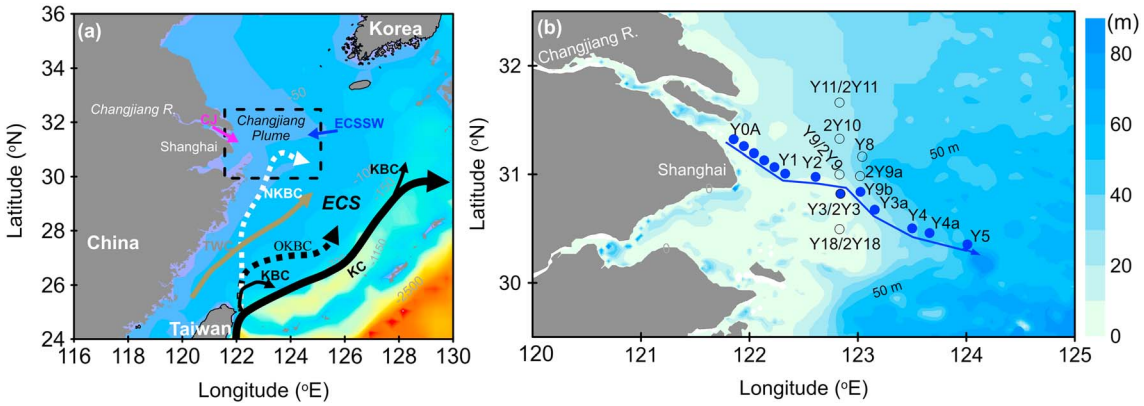

Figure 1. Maps of the East China Sea (ECS) and the Changjiang offshore: (a) Water circulation pattern in summer, modified from Yang et al. (2012). (b) Sampling stations with topography (as shown in color contours). In Figure 1a, the pink arrow indicates the main channel, the blue arrow represents the ECS Surface Water (ECSSW), the gray arrow is the Taiwan Warm Current (TWC), the black arrows are Kuroshio Current (KC) and Kuroshio Branch Current (KBC), the black dashed arrow is Offshore KBC (OKBC), and the white dashed arrow is the Nearshore KBC (NKBC) underlying the TWC. In Figure 1b, blow-up of the dashed square in Figure 1a, the transect (blue line) comprises stations (blue dots) from Y0A through Y5. Other stations were shown in black circles.

the relative importance of these NO_3^- sources from the CJ, the NKBC, and the remineralization beneath the plume?

To answer these questions and explore the N transformations in the CJ plume, we conducted a field program of depth-resolved sampling from the main channel of the river offshore across the shelf (Figure 1b). We measured the dual isotopic composition of NO_3^- ($\delta^{15}N_{NO3}$ and $\delta^{18}O_{NO3}$), which provides powerful insights into N transformation processes in complex estuarine and coastal systems (Möbius & Dähnke, 2015; Umezawa et al., 2014). In particular, it helps to identify the relative importance of NO_3^- removal (by phytoplankton assimilation in the euphotic zone or denitrification in the subsurface oxygen-deficient zone) versus NO_3^- supply by nitrification. This is because the removal processes occur with parallel enrichments in $\delta^{15}N_{NO3}$ and $\delta^{18}O_{NO3}$ (Deutsch et al., 2009; Korth et al., 2013; Sigman et al., 2003), whereas greater enrichment of $\delta^{18}O_{NO3}$ ($\delta^{18}O_{NO3}$:$\delta^{15}N_{NO3}$ = 1.2–1.6) accompanies nitrification (Dähnke et al., 2010; Ye et al., 2015).

We interpret the NO_3^- concentration and its dual isotope variations using a three end-member mixing model that allows us to distinguish biogeochemical transformations from circulation influences. Within the mixing model framework, we are able to assess the relative importance of these sources and processes. Accordingly, we constructed an overall conceptual framework for NO_3^- dynamics during the summer hypoxia period for the CJ plume, which is likely to have broader applicability and utility to coastal zones influenced by turbid N-rich river flows.

2. Materials and Methods

2.1. Study Area

The CJ plume is characterized by complex hydrodynamics during summer. The water in the plume is composed of multiple water sources (Figure 1a) including the CJ freshwater, ECS Surface Water (ECSSW), and NKBC water (Chen, 1996; Yang et al., 2012).

Our work builds on sparse previous efforts using the single $\delta^{15}N_{NO3}$ in the CJ plume. The first work by Liu et al. (2009) focused on surface waters and thus did not address identification of NO_3^- subsurface sources. Similar work by Yu et al. (2015), again lacking measurements of $\delta^{18}O_{NO3}$, was limited in its assessment of the influence of nitrification, a common process in coastal waters (Dähnke et al., 2010; Ye et al., 2015). The only dual isotope work in the CJ plume was conducted by Chen et al. (2013) in spring, a period during which active NO_3^- assimilation by phytoplankton is a dominant control. Our work represents the first attempt to unravel the multiple N sources and cycling processes within/below the CJ plume in summer.

2.2. Sampling

A cruise was conducted during 15–24 August 2011. A total of 19 stations were sampled to examine the spatial distributions of NO_3^- and its isotopic composition within the CJ plume (Figure 1b; stations Y3, Y9, Y11, and

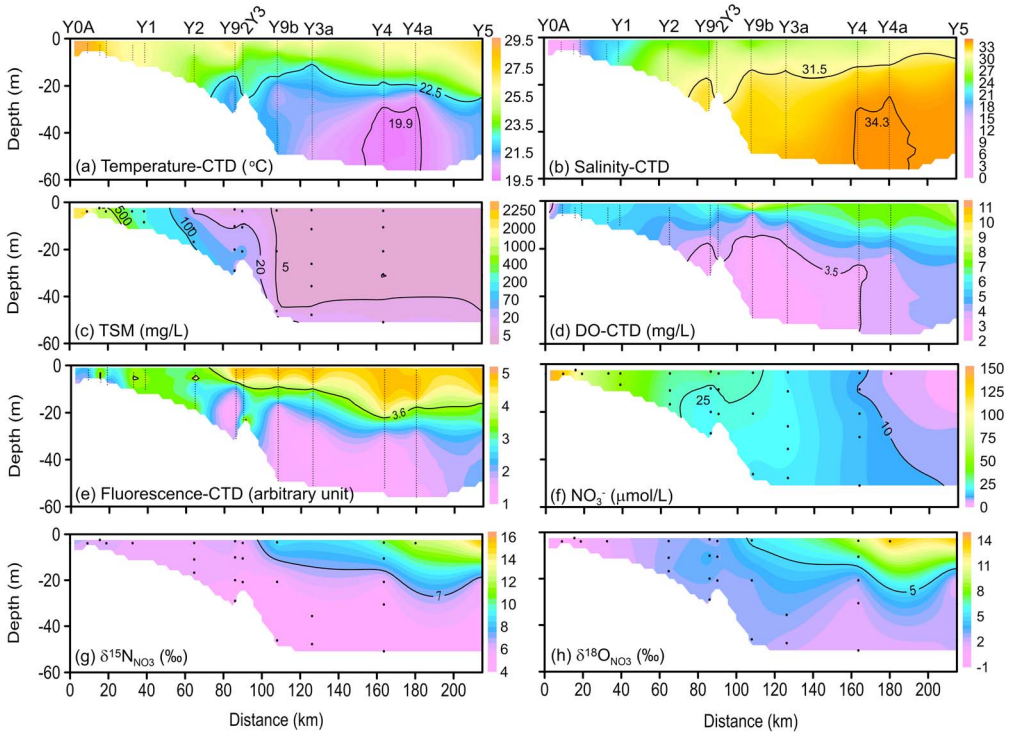

Figure 2. Transectional distributions of (a) temperature, (b) salinity, (c) TSM, (d) DO, (e) fluorescence, (f) NO_3^-, (g) $\delta^{15}N_{NO3}$, and (h) $\delta^{18}O_{NO3}$. Note that partial data of temperature, salinity, DO, TSM, and NO_3^- presented in Figures 2a, 2b, 2c, 2d, and 2f were reported elsewhere (Hsiao et al., 2014; Tseng et al., 2014).

Y18 were revisited). Water samples were collected using a rosette sampler fitted with 12 L Niskin bottles and a conductivity temperature depth (CTD) unit (SBE 911, Sea-Bird Co.). Vertical profiles of temperature, salinity, DO, and chlorophyll fluorescence were sampled at 3 Hz with the CTD lowered at 1 m/s. The CTD data were averaged at 1 m intervals for presentation. The water depth varied between 6 m in the river mouth to 63 m offshore.

2.3. Isotopic Analyses

Water samples for the isotopic composition of NO_x (NO_3^- + NO_2^-) were filtered through cellulose acetate membranes (0.45 μm pore size) and kept at −20°C until determination. Since NO_2^- contributed a small fraction of NO_x (2.5 ± 2.2%, n = 64, Table S1 in the supporting information), NO_x is referred to as NO_3^- hereafter. The isotopic composition of NO_3^- was measured using the denitrifier method (Casciott et al., 2002; Sigman et al., 2001). The analytical precisions for $\delta^{15}N_{NO3}$ and $\delta^{18}O_{NO3}$ of field samples were better than ±0.2‰ and ±0.5‰ (replicate measurements), respectively. Details of the isotopic analyses are in the supporting information (Text S1).

3. Results and Discussions

3.1. Spatial Distributions of Water Masses and Isotopic Composition

Water temperature along the transect ranged from 19.5 to 29.5°C with a strong thermal stratification and a low temperature core (<19.9°C) in the offshore bottom water (Figure 2a). A salt-wedge intrusion pattern was observed for salinity (Figure 2b). The low-temperature high-salinity core at the bottom at station Y4/Y4a (T < 19.9°C, S > 34.3) had T–S properties close to those of NKBC (T = 18°C, S = 34.4–34.6; Yang et al., 2012). High-temperature and high-salinity water was found near the fringe of the surface plume at station Y5, as influenced by the ECSSW (Wang et al., 2016).

Total suspended material (TSM) decreased from a high of >2,000 mg/L (Y0A) to 20 mg/L (2Y3) >100 km offshore. TSM was <5 mg/L in the whole outer plume, except for the bottom layers near shore (Figure 2c).

DO exhibited strong vertical variations, with the highest values at the surface in the outer plume and the lowest values at the bottom (Figure 2d). Note that the zone with the lowest DO (<3.5 mg/L) was well inshore from the center core of the NKBC. Chlorophyll fluorescence was highest in the offshore surface waters (Figure 2e), where stratification was strongest and turbidity lowest.

Concentrations of NO_3^- showed a seaward decreasing pattern (Figure 2f), with the highest value (150.5 μmol/L) in the river mouth and the lowest (4.2 μmol/L) in the surface layer at offshore station Y5. Moderate concentrations of NO_3^- appeared in the middle part of the transect (stations Y3a/Y4) with less vertical variations. The spatial distributions of *T*, *S*, and NO_3^- suggested that CJ and NKBC were two important NO_3^- source waters, diluted into the oligotrophic waters of the ECSSW.

Along the transect, distinctively high values of $\delta^{15}N_{NO3}$ (>7‰) and $\delta^{18}O_{NO3}$ (>5‰) were found in the offshore surface water (Figures 2g and 2h). The highest values ($\delta^{15}N_{NO3}$ of 15.9‰, $\delta^{18}O_{NO3}$ of 14.0‰) appeared in the very surface waters of station Y4a/Y5, where NO_3^- concentrations were lowest. These were accompanied by high chlorophyll fluorescence, implying active NO_3^- assimilation by phytoplankton. In comparison to the high isotope values in the surface layer, the $\delta^{15}N_{NO3}$ (4.9–6.0‰) and $\delta^{18}O_{NO3}$ (1.7–3.9‰) values of deeper waters and at the river mouth were both lower and less variable.

3.2. Identification of N Transformations in the CJ Plume

To examine the biological influences on NO_3^-, we applied a three end-member model (Álvarez-Salgado et al., 1997) to calculate water mixing ratios and thus the NO_3^- concentrations expected from the physical mixing alone (C_{ex}). Any deviations between observed and expected values ($C_{obs} - C_{ex}$, denoted as "NO_3-offset" hereafter; see vertical red lines in Figure S1b) represent biological alteration (i.e., in situ consumption or production). Following the same procedure, the isotope-offsets ($\delta^{15}N_{NO3}$-offset and $\delta^{18}O_{NO3}$-offset) can be obtained and used to identify the processes involved. Details of the end-member selection and the mixing calculations are provided in the SI (Text S2 and S3, Figure S1, and Table S2). This approach has been successfully applied to evaluate biological influences of macronutrients and carbonate system (Cao et al., 2011; Han et al., 2012).

To reveal NO_3^- sources and dynamics, we plotted the isotope-offsets versus the NO_3-concentration-offsets (Figures 3a and 3b). According to the distributions of data points in these plots, we classified the samples into three zones, representing specific N transformation processes. The three zones were Zone 1: the water-column nitrification and sedimentary denitrification; Zone 2: the remineralization–nitrification; and Zone 3: the assimilation. The information on the N transformation processes is presented spatially (Figures 3d–3f) and separated into three regions. We now discuss offsets in these zones, in terms of both identifying the main processes involved and semiquantifying them.

The Zone 1 compositions appeared mainly near the river mouth (Figures 3c–3f). In Zone 1, we can see obvious NO_3^- deficits (−0.2 to −12.5 μmol/L) accompanied by slightly negative $\delta^{15}N_{NO3}$-offsets (−0.1 to −0.6‰) and significantly positive $\delta^{18}O_{NO3}$-offsets (+3.0‰). As noted in the introduction, both assimilation and denitrification could explain NO_3^- loss. However, NO_3^- assimilation by phytoplankton should be limited by the high turbidity in Zone 1 (Figure 2c) although we cannot completely exclude this possibility since fluorescence was detectable. Yet from the investigation in the same cruise, both chlorophyll and APA were reported to be allochthonous (Tseng et al., 2014). Moreover, the DO concentrations (2.9–6.2 mg/L, Figure 2d) were sufficient to inhibit denitrification in the water column (Codispoti et al., 2001), supported by the undetectable denitrification rates within 24 h incubation (Text S4). Thus, the best explanation is loss of NO_3^- by sedimentary denitrification, which is consistent with the high denitrification rates previously observed in river mouth sediments (10–20 nmol/cm^3/h; Song et al., 2013). Sedimentary denitrification generally occurs with no isotope effect if all NO_3^- is consumed (Brandes & Devol, 1997; Lehmann et al., 2004); thus, it does not leave any signature in water-column $\delta^{15}N_{NO3}$ and $\delta^{18}O_{NO3}$. However, partial denitrification (i.e., with some release of NO_3^- to the water column due to the strong tidal mixing) could also occur in water–sediment interface, provided the associated increase of both $\delta^{15}N_{NO3}$ and $\delta^{18}O_{NO3}$ (Prokopenko et al., 2011). Nevertheless, the above increase of $\delta^{15}N_{NO3}$ was overwhelmed by the impact of water-column nitrification since it lowers $\delta^{15}N$ in regenerated NO_3^- (Sugimoto et al., 2009; Wankel et al., 2009). Active nitrification rates were observed in the water column near the turbid river mouth during the same voyage (Hsiao et al., 2014). Moreover, positive correlations were also observed among nitrification rate, TSM, and particle associated *amoA*-type nitrifying microorganisms (Zhang et al., 2014).

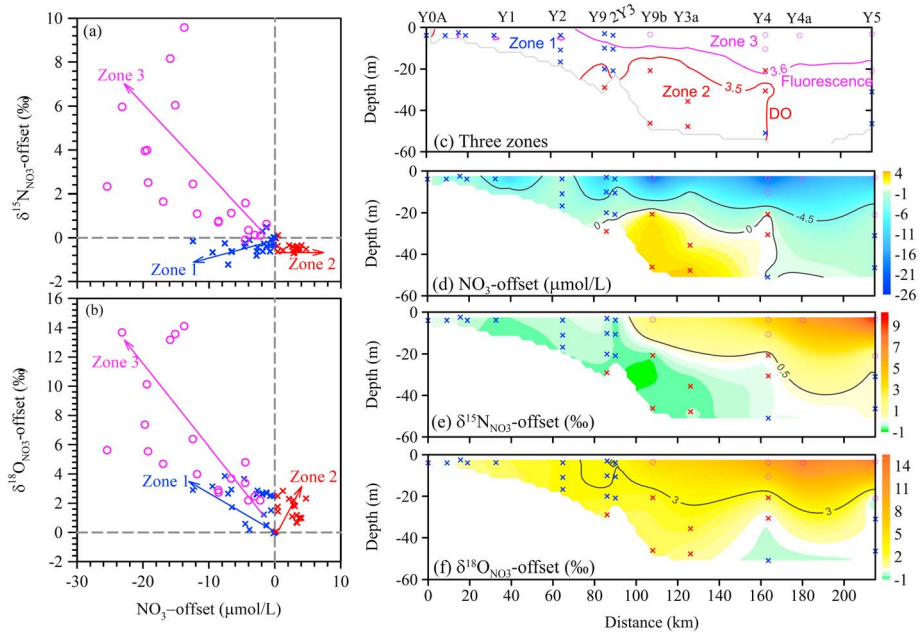

Figure 3. (left) The scatter plots for (a) $\delta^{15}N_{NO3}$-offset and (b) $\delta^{18}O_{NO3}$-offset versus NO_3-offset. (right) The distributions of (c) three zones, (d) NO_3-offset, (e) $\delta^{15}N_{NO3}$-offset, and (f) $\delta^{18}O_{NO3}$-offset. The blue crosses, red crosses, and pink circles are for Zone 1, Zone 2, and Zone 3, respectively. In Figure 3c, isopleths of fluorescence (pink, arbitrary unit) and DO (red, mg/L) were marked.

In summary, all observations categorize Zone 1 as dominated by water-column nitrification and sedimentary denitrification. The difference in the integrated effect of these processes is obviously given by the net decrease in NO_3^-. Using isotope mass balance, it is possible to go further and make an estimate of the nitrification/denitrification ratio. The required equations and details of assumptions, calculations, and error minimization are provided in the SI (Text S5). The result leads to an error minimization estimate of 0.60 for the nitrification/denitrification ratio. Thus, the 3.4 ± 3.2 μmol/L (n = 26) of NO_3^- deficit results from the combination of 8.4 ± 8.1 μmol/L denitrification loss and 5.0 ± 4.9 μmol/L nitrification gain, so that roughly in total ~35% of the NO_3^- present (38.8 ± 37.5 μmol/L) has been microbially transformed in Zone 1. Most importantly, the isotopic results make it unassailably clear that nitrification and denitrification strongly modulate the riverine NO_3^- source before it is dispersed offshore to fuel phytoplankton assimilation.

In Zone 2, the most distinctive feature was a patch of highly elevated NO_3^- near the bottom (Figure 3d). This distribution overlaid the low DO region (<3.5 mg/L, Figure 3c). In these waters, the $\delta^{15}N_{NO3}$-offsets ranged narrowly from −0.7 to −0.1‰ (Figure 3e), while the $\delta^{18}O_{NO3}$-offsets were significantly higher ranging from +0.1 to +2.8‰ (Figure 3f). The most plausible cause to support this excess NO_3^- and lower $\delta^{15}N_{NO3}$ was the remineralization and nitrification of particulates organic matter deposited from the upper layers. This notion is also supported by the $\delta^{13}C$ budget (Wang et al., 2016), demonstrating that the DO decrease in this zone was induced by the remineralization of autochthonous organics produced in the surface layer. Both the relatively long residence time of the bottom waters (~11days; Rabouille et al., 2008) and low DO levels (<3.5 mg/L) provide further evidence of organic matter remineralization.

In Zone 2, similarly to Zone 1, water-column denitrification could not be detected (Text S4), although DO values in Zone 2 were lower than those of Zone 1. Apparently, the lower DO values did not reach the threshold for water-column denitrification (<5 μmol/kg; Codispoti et al., 2001). Judging from the low TSM concentrations, the proposed mechanism for partial denitrification due to strong tidal mixing is unlikely in Zone 2. There may have been an influence from complete denitrification within the sediments, since it does not leave a signature in the water column of NO_3^- isotopic composition. Nevertheless, the same semiquantitative analysis for Zone 2 as conducted in Zone 1 suggests that the influence of complete denitrification from sediments was limited (nitrification/denitrification ratio > 2.2; Text S5 and Figure S3b).

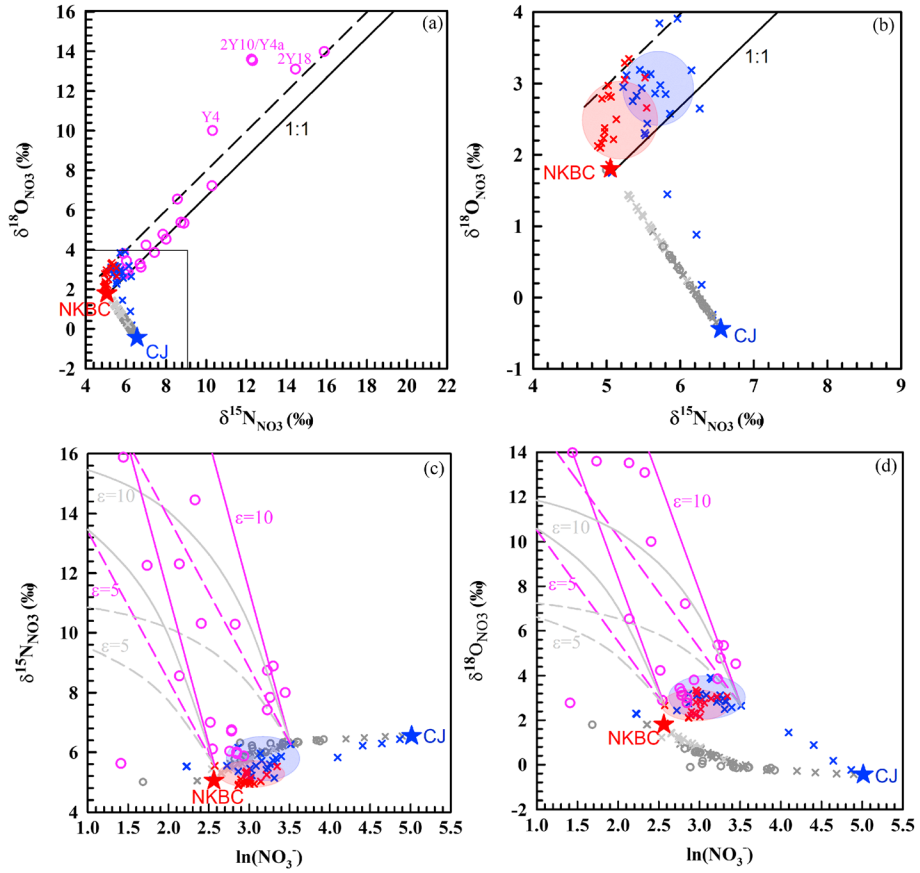

Figure 4. The scatter plots for (a) $\delta^{18}O_{NO3}$ versus $\delta^{15}N_{NO3}$, (b) blow-up of the rectangle in Figure 4a, (c) $\delta^{15}N_{NO3}$, and/or (d) $\delta^{18}O_{NO3}$ versus the natural logarithm of nitrate. Mixing-derived values were in gray symbols, indicating the mixing between NKBC (red star) and CJ (blue star). The black lines in Figures 4a and 4b indicate NO_3^- assimilation trends (line 1:1). The solid and dashed lines in Figures 4c and 4d indicate the expected shift in $\delta^{15}N_{NO3}$ (or $\delta^{18}O_{NO3}$) associated with NO_3^- assimilation following the Rayleigh model (pink lines) and the steady-state model (gray curves) by given isotope effect of 5‰ (dashed lines) and 10‰ (solid lines), respectively. Blue and red shade represent the fields of Zone 1 and Zone 2, respectively.

In Zone 3, the surface outer plume, significant NO_3^- deficits occurred (−4.5 to −25.5 μmol/L; Figure 3d) accompanied by positive $\delta^{15}N_{NO3}$-offsets (+0.5 to +9.6‰; Figure 3e) and $\delta^{18}O_{NO3}$-offsets (+2.2 to +14.1‰; Figure 3f). This suggests the dominance of the NO_3^- assimilation by phytoplankton, consistent with the high fluorescence (>3.6, arbitrary unit; Figure 3c). The relative enrichment of $\delta^{18}O_{NO3}$ and $\delta^{15}N_{NO3}$ displayed a linear trend of 1:1 (Figure 4a), also as expected for assimilation by phytoplankton (Granger et al., 2004, 2010; Karsh et al., 2014). However, several data points (Y4, Y4a, 2Y10, and 2Y18) deviated from the 1:1 line, which can be attributed to nitrification as producing a positive shift in $\delta^{18}O_{NO3}$ relative to $\delta^{15}N_{NO3}$ in recycled NO_3^- (Wankel et al., 2009). Similar phenomena were found in several field studies, such as the German Bight (Dähnke et al., 2010) and the Pearl River estuary (Ye et al., 2015). Alternatively, NO_3^- uptake by heterotrophic α-proteobacteria can also result in such deviation since it fractionates $\delta^{18}O_{NO3}$ and $\delta^{15}N_{NO3}$ unevenly with a slope of 2 (Granger et al., 2010).

The overall 1:1 correlation of dual isotope in Zone 3 suggests that the data may be used to deduce the isotope effect of phytoplankton assimilation, as done in previous studies (Möbius & Dähnke, 2015; Sigman et al., 1999). In doing this, it is important to note that the 1:1 linear trend (Figure 4b) did not originate from the CJ end-member or the mixing line of CJ and NKBC. It derives from a NO_3^- source with a narrow range of $\delta^{15}N_{NO3}$ and $\delta^{18}O_{NO3}$ (as shown in blue and red shade), representative of the microbially altered conditions in Zone 1 and Zone 2. This confirms that the NO_3^- utilized by phytoplankton growth may have been altered by microbial processes prior to assimilation. It counters the conventional thought that in surface river plumes,

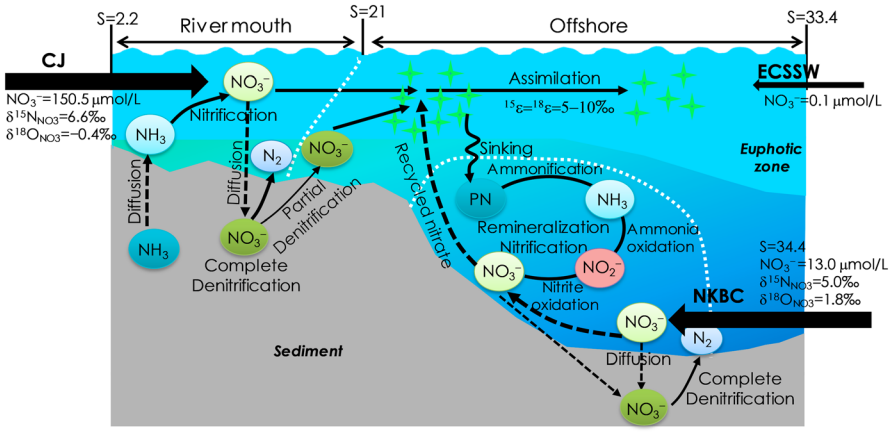

Figure 5. Conceptual diagram for nitrogen cycling in the CJ plume.

phytoplanktons use NO_3^- directly discharged from the major NO_3^- supplier, which in this case is the CJ. Although the mixing model suggests that the CJ dominates the NO_3^- inventory in the surface 15 m (>55%; Figure S2b), the NO_3^- for phytoplankton assimilation is actually a mixture of microbially transformed NO_3^- from Zone 1 and Zone 2. To further evaluate the relative contribution from the NKBC is difficult since the NKBC end-member fell close to the fields of Zone 1 and Zone 2.

After recognizing the importance of recycled NO_3^- as the source to fuel phytoplankton growth, we tried to estimate the isotope effects (ε) during assimilation (Sigman et al., 1999; Sugimoto et al., 2009). As shown in Figures 4c and 4d, the Zone 3 data are compatible with ε values ranging from 5‰ to 10‰, for either Rayleigh model or steady-state model, with the former more readily fitting the highest isotope values. These ε values fit well with results for diatom cultures (5–18‰; Granger et al., 2004; Needoba et al., 2003), and based on previous studies (Furuya et al., 2003; Liu et al., 2016), diatoms are indeed the dominant species in the CJ plume during summer. Overall, the data are too scattered to make precise estimate of ε values. Importantly, incorrectly low ε values would be inferred by connecting the Zone 3 assimilation process with the NO_3^- source composition from CJ.

3.3. Conceptual View of N Transformations in the CJ Plume

We summarize the multiple zones and overall N processing in the CJ plume in a conceptual diagram (Figure 5), showing the coupling of water-column nitrification and sedimentary denitrification near the river mouth, intensive remineralization and nitrification in the low-DO bottom water, and NO_3^- assimilation in the surface outer plume. This sequence of processing and zones is likely to occur in many river-impacted coastal systems, although their relative intensities may vary seasonally and yearly. The combination of mixing model and NO_3^- dual isotope to identify biogeochemical transformations, and their spatial localization relative to physical characteristics (such as riverine flows, bathymetry, and resuspension/turbidity), offers a powerful approach to broadening our understanding of the changing coastal zones. Use of this formalism is likely to allow an emerging picture to be resolved more rapidly, including both similarities and contrasts among different systems.

Acknowledgments
We are grateful for constructive comments from two anonymous reviewers. We thank Patricia M. Glibert and Todd Kana (University of Maryland Center for Environmental Science, USA) for useful comments and helpful edits on this manuscript. We thank Lin Jing and our colleagues at the State Key Laboratory of Marine Environmental Science (Xiamen University, China). We especially thank Zhao Huade and Qian Wei for their help in drawing 3-D plots. This research was supported by the National Natural Science Foundation of China (NSFC U1305233, 41561164019, 2015CB954003). This is the MEL contribution number #melpublication2017188. Data supporting this study are available in supporting information Table S1.

References

Altabet, M. A. (2006). Isotopic tracers of the marine nitrogen cycle: Present and past. In J. Volkman (Ed.), *Marine Organic Matter: Chemical and Biological Markers* (pp. 251–293). Berlin: Springer.

Álvarez-Salgado, X. A., Castro, C. G., PÉRez, F. F., & Fraga, F. (1997). Nutrient mineralization patterns in shelf waters of the western Iberian upwelling. *Continental Shelf Research*, *17*(10), 1247–1270. https://doi.org/10.1016/S0278-4343(97)00014-9

Anderson, D. M., Glibert, P. M., & Burkholder, J. M. (2002). Harmful algal blooms and eutrophication: Nutrient sources, composition, and consequences. *Estuaries*, *25*(4), 704–726. https://doi.org/10.1007/BF02804901

Billen, G., Garnier, J., Deligne, C., & Billen, C. (1999). Estimates of early-industrial inputs of nutrients to river systems: Implication for coastal eutrophication. *Science of the Total Environment*, *243-244*, 43–52. https://doi.org/10.1016/S0048-9697(99)00327-7

Böhlke, J. K., Mroczkowski, S. J., & Coplen, T. B. (2003). Oxygen isotopes in nitrate: New reference materials for ^{18}O:^{17}O:^{16}O measurements and observations on nitrate–water equilibration. *Rapid Communications in Mass Spectrometry*, *17*(16), 1835–1846. https://doi.org/10.1002/rcm.1123

Brandes, J. A., & Devol, A. H. (1997). Isotopic fractionation of oxygen and nitrogen in coastal marine sediments. *Geochimica et Cosmochimica Acta*, *61*(9), 1793–1801. https://doi.org/10.1016/S0016-7037(97)00041-0

Buchwald, C., & Casciotti, K. L. (2010). Oxygen isotopic fractionation and exchange during bacterial nitrite oxidation. *Limnology and Oceanography*, *55*, 1064–1074. https://doi.org/10.4319/lo.2010.55.3.1064

Buchwald, C., Santoro, A. E., McIlvin, M. R., & Casciotti, K. L. (2012). Oxygen isotopic composition of nitrate and nitrite produced by nitrifying cocultures and natural marine assemblages. *Limnology and Oceanography*, *57*, 1361–1375. https://doi.org/10.4319/lo.2012.57.5.1361

Cao, Z., Dai, M., Zheng, N., Wang, D., Li, Q., Zhai, W., … Gan, J. (2011). Dynamics of the carbonate system in a large continental shelf system under the influence of both a river plume and coastal upwelling. *Journal of Geophysical Research*, *116*, G02010. https://doi.org/10.1029/2010JG001596

Casciott, K. L., Sigman, D. M., Hastings, M. G., Bohlke, J. K., & Hilkert, A. (2002). Measurement of the oxygen isotopic composition of nitrate in seawater and freshwater using the denitrifier method. *Analytical Chemistry*, *74*(19), 4905–4912. https://doi.org/10.1021/ac020113w

Chen, C.-T. A. (1996). The Kuroshio intermediate water is the major source of nutrients on the East China Sea continental shelf. *Oceanologica Acta*, *19*(5), 523–527.

Chen, F., Chen, J., Jia, G., Jin, H., Xu, J., Yang, Z., … Zhang, H. (2013). Nitrate $\delta^{15}N$ and $\delta^{18}O$ evidence for active biological transformation in the Changjiang estuary and the adjacent East China Sea. *Acta Oceanologica Sinica*, *32*(4), 11–17. https://doi.org/10.1007/s13131-013-0294-4

Codispoti, L. A., Brandes, J. A., Christensen, J. P., Devol, A. H., Naqvi, S. W. A., Paerl, H. W., & Yoshinari, T. (2001). The oceanic fixed nitrogen and nitrous oxide budgets: Moving targets as we enter the Anthropocene? *Scientia Marina*, *65*(S2), 85–105. https://doi.org/10.3989/scimar.2001.65s285

Dähnke, K., Emeis, K., Johannsen, A., & Nagel, B. (2010). Stable isotope composition and turnover of nitrate in the German Bight. *Marine Ecology Progress Series*, *408*, 7–18. https://doi.org/10.3354/meps08558

Dai, Z. J., Du, J. Z., Zhang, X. L., Su, N., & Li, J. F. (2011). Variation of riverine material loads and environmental consequences on the Changjiang (Yangtze) estuary in recent decades (1955–2008). *Environmental Science & Technology*, *45*, 223–227. https://doi.org/10.1021/es103026a

Deutsch, B., Voss, M., & Fischer, H. (2009). Nitrogen transformation processes in the Elbe River: Distinguishing between assimilation and denitrification by means of stable isotope ratios in nitrate. *Aquatic Sciences*, *71*, 228–237. https://doi.org/10.1007/s00027-009-9147-9

Diaz, R. J., & Rosenberg, R. (2008). Spreading dead zones and consequences for marine ecosystem. *Science*, *321*(5891), 926–929. https://doi.org/10.1126/science.1156401

Furuya, K., Hayashi, M., Yabushita, Y., & Ishikawa, A. (2003). Phytoplankton dynamics in the East China Sea in spring and summer as revealed by HPLC-derived pigment signatures. *Deep Sea Research Part II*, *50*(2), 367–387. https://doi.org/10.1016/S0967-0645(02)00460-5

Granger, J., Sigman, D. M., Needoba, J. A., & Harrison, P. J. (2004). Coupled nitrogen and oxygen isotope fractionation of nitrate during assimilation by cultures of marine phytoplankton. *Limnology and Oceanography*, *49*, 1763–1773. https://doi.org/10.4319/lo.2004.49.5.1763

Granger, J., Sigman, D. M., Rohde, M. M., Maldonado, M. T., & Tortell, P. D. (2010). N and O isotope effects during nitrate assimilation by unicellular prokaryotic and eukaryotic plankton cultures. *Geochimica et Cosmochimica Acta*, *74*, 1030–1040. https://doi.org/10.1016/j.gca.2009.10.044

Gruber, N., & Galloway, J. N. (2008). An Earth-system perspective of the global nitrogen cycle. *Nature*, *451*, 293–296. https://doi.org/10.1038/nature06592

Han, A., Dai, M., Kao, S.-J., Gan, J., Li, Q., Wang, L., … Wang, L. (2012). Nutrient dynamics and biological consumption in a large continental shelf system under the influence of both a river plume and coastal upwelling. *Limnology and Oceanography*, *57*, 486–502. https://doi.org/10.4319/lo.2012.57.2.0486

Hsiao, S. S.-Y., Hsu, T. C., Liu, J.w., Xie, X., Zhang, Y., Lin, J., … Kao, S. J. (2014). Nitrification and its oxygen consumption along the turbid Chang Jiang River plume. *Biogeosciences*, *11*(7), 2083–2098. https://doi.org/10.5194/bg-11-2083-2014

Karsh, K. L., Trull, T. W., Sigman, D. M., Thompson, P. A., & Granger, J. (2014). The contributions of nitrate uptake and efflux to isotope fractionation during algal nitrate assimilation. *Geochimica et Cosmochimica Acta*, *132*, 391–412. https://doi.org/10.1016/j.gca.2013.09.030

Korth, F., Fry, B., Liskow, I., & Voss, M. (2013). Nitrogen turnover during the spring outflows of the nitrate-rich Curonian and Szczecin lagoons using dual nitrate isotopes. *Marine Chemistry*, *154*, 1–11. https://doi.org/10.1016/j.marchem.2013.04.012

Lehmann, M. F., Sigman, D. M., & Berelson, W. M. (2004). Coupling the $^{15}N/^{14}N$ and $^{18}O/^{16}O$ of nitrate as a constraint on benthic nitrogen cycling. *Marine Chemistry*, *88*, 1–20. https://doi.org/10.1016/j.marchem.2004.02.001

Li, H.-M., Tang, H.-J., Shi, X.-Y., Zhang, C.-S., & Wang, X.-L. (2014). Increased nutrient loads from the Changjiang (Yangtze) River have led to increased harmful algal blooms. *Harmful Algae*, *39*, 92–101. https://doi.org/10.1016/j.hal.2014.07.002

Liu, X., Xiao, W., Landry, M. R., Chiang, K.-P., Wang, L., & Huang, B. (2016). Responses of phytoplankton communities to environmental variability in the East China Sea. *Ecosystems*, *19*(5), 832–849. https://doi.org/10.1007/s10021-016-9970-5

Liu, X., Yu, Z., Song, X., & Cao, X. (2009). The nitrogen isotopic composition of dissolved nitrate in the Yangtze River (Changjiang) estuary, China. *Estuarine, Coastal and Shelf Science*, *85*(4), 641–650. https://doi.org/10.1016/j.ecss.2009.09.017

Möbius, J., & Dähnke, K. (2015). Nitrate drawdown and its unexpected isotope effect in the Danube estuarine transition zone. *Limnology and Oceanography*, *60*(3), 1008–1019. https://doi.org/10.1002/lno.10068

Moore, C. M., Mills, M. M., Arrigo, K. R., Berman-Frank, I., Bopp, L., Boyd, P. W., … Ulloa, O. (2013). Processes and patterns of oceanic nutrient limitation. *Nature Geoscience*, *6*(9), 701–710. https://doi.org/10.1038/ngeo176

Needoba, J. A., Waser, N. A., Harrison, P. J., & Calvert, S. (2003). Nitrogen isotope fractionation in 12 species of marine phytoplankton during growth on nitrate. *Marine Ecology Progress Series*, *255*, 81–91. https://doi.org/10.3354/meps255081

Prokopenko, M. G., Sigman, D. M., Berelson, W. M., Hammond, D. E., Barnett, B., Chong, L., & Townsend-Small, A. (2011). Denitrification in anoxic sediments supported by biological nitrate transport. *Geochimica et Cosmochimica Acta*, *75*, 7180–7199. https://doi.org/10.1016/j.gca.2011.09.023

Qian, W., Dai, M., Xu, M., Kao, S. J., Du, C., Liu, J., … Wang, L. (2016). Non-local drivers of the summer hypoxia in the East China Sea off the Changjiang estuary. *Estuarine, Coastal and Shelf Science*, *198*, 393–399. https://doi.org/10.1016/j.ecss.2016.08.032

Rabouille, C., Conley, D. J., Dai, M. H., Cai, W. J., Chen, C. T. A., Lansard, B., … McKee, B. (2008). Comparison of hypoxia among four river-dominated ocean margins: The Changjiang (Yangtze), Mississippi, Pearl, and Rhône rivers. *Continental Shelf Research*, *28*, 1527–1537. https://doi.org/10.1016/j.csr.2008.01.020

Santoro, A. E., & Casciotti, K. L. (2011). Enrichment and characterization of ammonia-oxidizing Archaea from the open ocean: Phylogeny, physiology and stable isotope fractionation. *The ISME Journal*, *5*(11), 1796–1808. https://doi.org/10.1038/ismej.2011.58

Sharples, J., Middelburg, J. J., Fennel, K., & Jickells, T. D. (2017). What proportion of riverine nutrients reaches the open ocean? *Global Biogeochemical Cycles*, *31*, 39–58. https://doi.org/10.1002/2016GB005483

Sigman, D. M., Altabet, M. A., McCorkle, D. C., Francois, R., & Fischer, G. (1999). The $\delta^{15}N$ of nitrate in the Southern Ocean: Consumption of nitrate in surface waters. *Global Biogeochemical Cycles*, *13*(4), 1149–1166. https://doi.org/10.1029/1999GB900038

Sigman, D. M., Casciott, K. L., Andreani, M., Barford, C., Galanter, M. B., & J. K. (2001). A bacterial method for the nitrogen isotopic analysis of nitrate in seawater and freshwater. *Analytical Chemistry*, *73*(17), 4145–4153. https://doi.org/10.1021/ac010088e

Sigman, D. M., Karsh, K. L., & Casciotti, K. L. (2009). Ocean process tracers: Nitrogen isotopes in the ocean. *Encyclopedia of Ocean Sciences*, 40–54.

Sigman, D. M., Robinson, R., Knapp, A. N., van Geen, A., McCorkle, D. C., Brandes, J. A., & Thunell, R. C. (2003). Distinguishing between water column and sedimentary denitrification in the Santa Barbara Basin using the stable isotopes of nitrate. *Geochemistry, Geophysics, Geosystems*, *4*(5), 1040. https://doi.org/10.1029/2002GC000384

Song, G. D., Liu, S. M., Marchant, H., Kuypers, M. M. M., & Lavik, G. (2013). Anammox, denitrification and dissimilatory nitrate reduction to ammonium in the East China Sea sediment. *Biogeosciences*, *10*(11), 6851–6864. https://doi.org/10.5194/bg-10-6851-2013

Sugimoto, R., Kasai, A., Miyajima, T., & Fujita, K. (2009). Transport of oceanic nitrate from the continental shelf to the coastal basin in relation to the path of the Kuroshio. *Continental Shelf Research*, *29*, 1678–1688. https://doi.org/10.1007/BF02374138

Tseng, Y.-F., Lin, J., Dai, M., & Kao, S.-J. (2014). Joint effect of freshwater plume and coastal upwelling on phytoplankton growth off the Changjiang River. *Biogeosciences*, *11*(2), 409–423. https://doi.org/10.5194/bg-11-409-2014

Umezawa, Y., Yamaguchi, A., Ishizaka, J., Hasegawa, T., Yoshimizu, C., Tayasu, I., … Yamawaki, N. (2014). Seasonal shifts in the contributions of the Changjiang River and the Kuroshio Current to nitrate dynamics in the continental shelf of the northern East China Sea based on a nitrate dual isotopic composition approach. *Biogeosciences*, *11*(4), 1297–1317. https://doi.org/10.5194/bg-11-1297-2014

Wang, H., Dai, M., Liu, J., Kao, S.-J., Zhang, C., Cai, W.-J., … Sun, J. (2016). Eutrophication-driven hypoxia in the East China Sea off the Changjiang estuary. *Environmental Science & Technology*, *50*(5), 2255–2263. https://doi.org/10.1021/acs.est.5b06211

Wankel, S. D., Kendall, C., & Paytan, A. (2009). Using nitrate dual isotopic composition ($\delta^{15}N$ and $\delta^{18}O$) as a tool for exploring sources and cycling of nitrate in an estuarine system: Elkhorn Slough, California. *Journal of Geophysical Research*, *114*, G01011. https://doi.org/10.1029/2008JG000729

Wu, Y., Zhang, J., Zhang, Z. F., Ren, J. L., & Cao, J. P. (2002). Seasonal variability of stable carbon and nitrogen isotope of suspended particulate matter in the Changjiang River (in Chinese). *Oceanologia et Limnologia Sinica*, *33*(5), 546–552.

Yang, D., Yin, B., Liu, Z., Bai, T., Qi, J., & Chen, H. (2012). Numerical study on the pattern and origins of Kuroshio branches in the bottom water of southern East China Sea in summer. *Journal of Geophysical Research*, *117*, C02014. https://doi.org/10.1029/2011JC007528

Ye, F., Ni, Z., Xie, L., Wei, G., & Jia, G. (2015). Isotopic evidence for the turnover of biological reactive nitrogen in the Pearl River estuary, south China. *Journal of Geophysical Research: Biogeosciences*, *120*, 661–672. https://doi.org/10.1002/2014JG002842

Yu, H., Yu, Z., Song, X., Cao, X., Yuan, Y., & Lu, G. (2015). Seasonal variations in the nitrogen isotopic composition of dissolved nitrate in the Changjiang River estuary, China. *Estuarine, Coastal and Shelf Science*, *155*, 148–155. https://doi.org/10.1016/j.ecss.2015.01.017

Zhang, Y., Xie, X., Jiao, N., Hsiao, S. S. Y., & Kao, S. J. (2014). Diversity and distribution of amoA-type nitrifying and nirS-type denitrifying microbial communities in the Yangtze River estuary. *Biogeosciences*, *11*(8), 2131–2145. https://doi.org/10.5194/bg-11-2131-2014

Zhu, Z.-Y., Zhang, J., Wu, Y., Zhang, Y.-Y., Lin, J., & Liu, S.-M. (2011). Hypoxia off the Changjiang (Yangtze River) estuary: Oxygen depletion and organic matter decomposition. *Marine Chemistry*, *125*, 108–116. https://doi.org/10.1016/j.marchem.2011.03.005